Nanostructured Hybrid Solar Cells Based on Self-Assembled Mesoporous Titania Thin Films

Emmanuelle Lancelle-Beltran,[†] Philippe Prené,*[,†] Christophe Boscher,[†] Philippe Belleville,[†] Pierrick Buvat,[†] Sébastien Lambert,[†] François Guillet,[†] Cédric Boissière,[‡] David Grosso,[‡] and Clément Sanchez*[,‡]

CEA−Le Ripault, BP 16, 37260 Monts, France, and Laboratoire de Chimie de la Matière Condensée, CNRS UMR7574, Université Pierre et Marie Curie, 4 place Jussieu, 75252 Paris Cedex 05, France

Received April 21, 2006. Revised Manuscript Received September 25, 2006

Nanocrystalline mesostructured porous titania thin films with optimized coating and thermal curing conditions have been prepared for the first time using spin-coating deposition technique. The X-ray diffraction (XRD) and the grazing incidence small-angle X-ray scattering (GI-SAXS) measurements revealed that the crystallization and diffuse sintering of amorphous TiO_2 into anatase are simultaneously starting between 400 and 500 °C curing temperature, leading to a gridlike open-pore-shape transformation. The environmental ellipsometric porosimetry (EEP) measurements show that the 550 °C-cured TiO_2 films exhibit a high porous volume (0.30 $cm^3\ g^{-1}$), a large surface area (172 $m^2\ cm^{-3}$), and a Young modulus of 1.05 GPa. All solid-state dye-sensitized solar cells (DSSC) based on nanocrystalline mesostructured TiO_2 films and poly(3-octylthiophene) as hole conductor allow reproducible achievement of energy conversion efficiencies of about 0.52%. These values, obtained with thin TiO_2 films (250 nm), are very promising.

Introduction

Currently, the dye-sensitized solar cells (DSSC) are a technical and economical alternative to the conventional silicon-based P−N junction photovoltaic devices.[1] Such cells based on a transparent nanocrystalline mesoporous TiO_2 layer as semiconductor, ruthenium-based complexes as dye, and an iodide/iodine redox couple in acetonitrile liquid as electrolyte allow high solar conversion efficiency level (over 10% at standard AM 1.5) with good durability to be obtained.[2,3] Even if DSSC devices are to date commercially available, market expansion did not take place because of technological issues induced by the use of highly corrosive liquid electrolytes (cell sealing, handling, and maintenance). Therefore, all solid-state dye-sensitized solar cells have been developed, replacing the liquid electrolyte with hole-transporting materials such as ionically conductive gels,[4] inorganic p-type conductors,[5,6] or molecular and macromolecular organic hole-conductive polymers.[7−31] While the energy conversion efficiency of all solid-state dye-sensitized solar cells, based on ionically conductive gels or inorganic p-type conductors, can reach 4%,[7] the use of organic hole-transporting materials leads commonly to a sudden drop of

* To whom correspondence should be addressed. P. Prené: tel., +33 2 47 34 55 87; fax, +33 2 47 34 56 76; e-mail, philippe.prene@cea.fr. C. Sanchez: e-mail, clems@ccr.jussieu.fr.

[†] CEA-Le Ripault.

[‡] CNRS UMR7574, Université Pierre et Marie Curie.

(1) O'Regan, B.; Grätzel, M. *Nature* **1991**, *353*, 737.
(2) Nazeeruddin, M. K.; Kay, A.; Rodicio, I.; Humphry-Baker, R.; Müller, E.; Liska, P.; Vlachopoulos, N.; Grätzel, M. *J. Am. Chem. Soc.* **1993**, *115*, 6382.
(3) Grätzel, M. *J. Photochem. Photobiol., A* **2004**, *164*, 3.
(4) Wang, P.; M. Zakeeruddin, S.; Comte, P.; Exnar, I.; Grätzel, M. *J. Am. Chem. Soc.* **2003**, *125*, 1166.
(5) Meng, Q. B.; Takahashi, K.; Zhang, X. T.; Sutanto, I.; Rao, T. N.; Sato, O.; Fujishima, A. *Langmuir* **2003**, *19*, 3572.
(6) O'Regan, B.; Lenzmann, F.; Muis, R.; Wienke, J. *Chem. Mater.* **2003**, *14*, 5023.
(7) Nogueira, A. F.; Longo, C.; De Paoli, M. A. *Coord. Chem. Rev.* **2004**, *248*, 1455.
(8) Krüger, J.; Plass, R.; Cevey, L.; Piccirelli, M.; Grätzel, M. *Appl. Phys. Lett.* **2001**, *79*, 2085.
(9) O'Regan, B.; Grätzel, M.; Zakeeruddin, S. M.; Grätzel, M. *Adv. Mater.* **2000**, *12*, 1263.
(10) Slooff, L. H.; Wienk, M. M.; Kroon, J. M. *Thin Solid Films* **2004**, *451*−452, 634.
(11) Kwong, C. Y.; Djurisic, A. B.; Chui, P. C.; Cheng, K. W.; Chan, W. K. *Chem. Phys. Lett.* **2004**, *384*, 372.
(12) Kumara, G. R. A.; Konno, A.; Shiratsushi, K.; Tsukahara, J.; Tennakone, K. *Chem. Mater.* **2002**, *14*, 954.
(13) Tennakone, K.; Kumara, G. R. A.; Kumarasinghe, A. R.; Wijayantha, K. G. U.; Sirimanne, P. M. *Sci. Technol.* **1995**, *10*, 1689.
(14) Tennakone, K.; Kumara, G. R. A.; Kottegoda, I. R. M.; Wijayantha, K. G. U.; Perera, V. P. S. *J. Phys. D: Appl. Phys.* **1998**, *31*, 1492.
(15) O'Regan, B.; Schwartz, D. T. *Chem. Mater.* **1995**, *7*, 1349.
(16) Hagen, J.; Schaffrath, W.; Otschik, P.; Fink, R.; Bacher, A.; Schmidt, H. W.; Haarer, D. *Synth. Met.* **1997**, *89*, 215.
(17) Ravirajan, P.; Bradley, D. D. C.; Nelson, J.; Haque, S. A.; Durrant, J. R.; Smit, H. J. P.; Kroon, J. M. *Appl. Phys. Lett.* **2005**, *86*, 143101-1.
(18) Gebeyehu, D.; Brabec, C. J.; Sariciftci, N. S. *Thin Solid Films* **2002**, *403*−*404*, 271.
(19) Gebeyehu, D.; Brabec, C. J.; Sariciftci, N. S.; Vangeneugden, D.; Kiebooms, R.; Vanderzande, D.; Kienberger, F.; Schindler, H. *Synth. Met.* **2002**, *125*, 279.
(20) Huisman, C. L.; Goossens, A.; Schoonman, J. *Synth. Met.* **2003**, *138*, 237.
(21) Grant, C. D.; Schwartzberg, A. M.; Smestad, G. P.; Kowalik, J.; Tolbert, L. M.; Zhang, J. Z. *Synth. Met.* **2003**, *132*, 197.
(22) Spiekermann, S.; Smestad, G.; Kowalik, J.; Tolbert, L. M.; Grätzel, M. *Synth. Met.* **2001**, *121*, 1603.
(23) Zafer, C.; Karapire, C.; Sariciftci, N. S.; Icli, S. *Sol. Energy Mater. Sol. Cells* **2005**, *88*, 11.
(24) Coakley, K. M.; McGehee, M. D. *Appl. Phys. Lett.* **2003**, *83*, 3380.
(25) Coakley, K. M.; McGehee, M. D. *Chem. Mater.* **2004**, *16*, 4533.
(26) Fan, Q.; McQuillin, B.; Bradley, D. D. C.; Whitelegg, S.; Seddon, A. B. *Chem. Phys. Lett.* **2000**, *347*, 325.
(27) Sirimanne, P. M.; Shirata, T.; Damodare, L.; Hayashi, Y.; Soga, T.; Jimbo, T. *Sol. Energy Mater. Sol. Cells* **2003**, *77*, 15.

10.1021/cm060925z CCC: $33.50
Published on Web 11/30/2006

solar device performances (typically below 1%).[9−32] The major problem associated with all solid-state dye-sensitized hybrid solar cells seems to be the filling of the porous TiO_2 film by the hole-transporting organic material.[7,22] Today, synthesis routes using block copolymers-based surfactants were proposed to prepare mesoporous TiO_2 layers with templated pore size and controlled porosity structures.[33−39] The porous TiO_2 layer in the dye-sensitized solar cells must exhibit efficient connectivities between nanocrystals to ensure the electron transfer to the collector electrode, extremely high surface area to increase the electron−hole pair density generated at the hybrid interface, and large open pores to promote hole-transporting organic material impregnation. Consequently, the tuning of TiO_2-films mesoporosity parameters such as pore size and connectivity, wall thickness, and crystallinity appears to be an attractive approach to better understand the physical and chemical parameters that control the efficiency of all solid-state dye-sensitized solar cells. Recently, dye-sensitized solar cells based on liquid electrolytes have been fabricated from mesostructured titania films.[40] These experiments performed with liquid-state electrolyte are very promising. Indeed, the results indicate that these solar cells exhibited a energy conversion efficiency (up to 5.31%) comparable to that of nanocrystalline colloidal anatase−TiO_2 films with the same thickness. Liquid and all solid-state dye-sensitized solar devices based on inverse TiO_2 opals using latex spheres template have also been investigated, but very low performances have been reported.[41,33]

In the present work, mesostructured nanocrystalline titania films prepared are made of periodically arranged anatase nanocrystals with well-defined crystal−crystal interfaces, compactly distributed around well-calibrated large mesopores. The films were prepared by sol−gel using an organic block copolymer template able to self-structure the films in organized mesodomains. The object of this paper was to evaluate the performances of all solid-state dye-sensitized solar cells based on regioregular poly(3-octylthiophene) as hole conductor as a function of the mesostructure and crystallinity of the porous TiO_2 film.

Experimental Section

The anhydrous titanium tetrachloride (i.e., $TiCl_4$), the block copolymer surfactant (Pluronic F_{127}, i.e., $HO(CH_2CH_2O)_{106}(CHCH_3CH_2O)_{70}(CH_2CH_2O)_{106}H$), and the regioregular poly(3-octylthiophene) (P3OT) were obtained from Aldrich and used as received ($M_w \sim 142000$, conductivity $= 10^{-6}$ S cm^{-1}). The Ru-based complex dye (II) ($RuL_2(NCS)_2$:2TBA, i.e., *cis*-bis(isothiocyanato)-bis(2,2′-bipyridyl-4,4′-dicarboxylato)ruthenium) was provided by Solaronix SA.

Preparation of Coating Solution. The coating solutions used for titania film deposition were synthesized as follows: a stock solution of titanium precursor was prepared by slowly adding $TiCl_4$ into ethanol (EtOH) under vigorous stirring at 0 °C. The typical molar ratio $TiCl_4$:EtOH was 1:5. As soon as the reagents were mixed, an exothermic reaction takes place, corresponding to $TiCl_2(OEt)_2$ yellow complex formation with HCl excess release. The typical coating solution was prepared by adding the titanium-based solution into a mixture of ethanol and the Pluronic F_{127} block copolymer surfactant, with the final molar ratio of 1:25:0.005 $TiCl_4$:EtOH:F_{127}.

Film Preparation. The films were deposited by spin coating onto silicon wafer, silica substrate, or fluorine-doped tin oxide (SnO_2:F) electrode covered glass substrate with an angular speed of 2000 rpm in a 100-class clean room. The relative humidity (RH) and the temperature during the deposition period were carefully controlled respectively at 45 ± 5 % and at 20 ± 1°C. After a drying step for a few minutes, the films were aged for 48 h in a RH-controlled atmosphere (50−60%) at room temperature. Finally, the films were sintered in air at different temperatures between 250 and 600 °C (ramp of 20 °C min^{-1}) for 30 min to remove the block copolymer surfactant and to sinter the titania network. The final film thickness is easily controlled from 10 to 300 nm by varying the coating speed.

Solid Hybrid Solar Cells Elaboration. After a sintering step, the TiO_2 electrodes were dye-coated by soaking them for 24 h in a dry ethanol-based solution of $RuL_2(NCS)_2$:2TBA dye (5×10^{-4} M) at room temperature in the dark. The dye-coated films were then rinsed with dry ethanol and dried in the dark under argon flow. The hole-transport layer was immediately coated by spin coating (500 rpm) from a P3OT solution in toluene (20 g L^{-1}). Finally, a 300-nm thickness gold back electrode was deposited onto the organic semiconductor film by sputtering. The thickness of the P3OT layer on top of the TiO_2 porous film was typically in the range of 100−200 nm as determined by Dektak profilometer measurements.

Characterization Techniques. In situ grazing incidence small-angle X-ray scattering (GI-SAXS) investigations were performed at the third generation synchrotron light source ELETTRA (Trieste, Italy) using a wavelength of 1.54 Å (8 keV). The glancing incidence was arbitrarily set at a value of 0.2°. The different patterns were recorded with a CCD detector (1024×1024 pixels, Photonic Science, 10 s acquisition). The sample was heated using a rate of 20 °C min^{-1} up to 550 °C. The glancing incident wide-angle X-ray diffraction (XRD) measurements were performed at room temperature on an INEL G3000 powder diffractometer (fixed incidence geometry), equipped with a flat Ge(111) monochromator (Cu $K\alpha_1$; $\lambda = 1.54056$ Å) and a curved position detector (INEL CPS 590). The incidence angle ω was set up to separate the scattered beams and the reflected beam ($\omega = 1.4°$). The transmission electron microscopy (TEM) images in ordinary resolution were collected using a JEOL 100CX II (120 kV). Samples were obtained by scratching the films from the substrate and then were suspended in

(28) Roberson, L. B.; Poggi, M. A.; Kowalik, J.; Smestad, G. P.; Bottomley, L. A.; Tolbert, L. M. *Coord. Chem. Rev.* **2004**, *248*, 1491.
(29) Breeze, A. J.; Schlesinger, Z.; Carter, S. A.; Brock, P. J. *Phys. Rev. B* **2001**, *64*, 125205.
(30) van Hal, P. A.; Wienk, M. M.; Kroon, J. M.; Verhees, W. J.; Sloof, L. H.; van Gennip, J. H.; Jonkheijm, P.; Janssen, R. A. J. *Adv. Mater. (Weinheim, Germany)* **2003**, *15*, 118.
(31) Song, M. Y.; Kim, K. J.; Kim, D. Y. *Sol. Energy Mater. Sol. Cells* **2005**, *85*, 31.
(32) Grant, C. D.; Schwartzberg, A. M.; Smestad, G. P.; Kowalik, J.; Tolbert, L. M.; Zhang, J. Z. *J. Electroanal. Chem.* **2002**, *522*, 40.
(33) Coakley, K. M.; Liu, Y.; McGehee, M. D.; Frindell, K. L.; Stucky, G. D. *Adv. Funct. Mater.* **2003**, *13*, 301.
(34) Kavan, L.; Rathousky, J.; Grätzel, M.; Shklover, V.; Zukal, A. *Microporous Mesoporous Mater.* **2001**, *44*−45, 653.
(35) Yang, P. D.; Zhao, D. Y.; Margolese, D. I.; Chmelka, B. F.; Stucky, G. D. *Nature (London)* **1998**, *396*, 152.
(36) Soler-Illia, G. J. A. A.; Sanchez, C.; Lebeau, B.; Patarin, J. *Chem. Rev.* **2002**, *102*, 4093.
(37) Soler-Illia, G. J. A. A.; Sanchez, C. *New J. Chem.* **2000**, *24*, 493.
(38) Crepaldi, E. L.; Soler-Illia, G. J. A. A.; Grosso, D.; Cagnol, F.; Ribot, F.; Sanchez, C. *J. Am. Chem. Soc.* **2003**, *125*, 9770.
(39) Zhao, L.; Yu, Y.; Song, L.; Ruan, M.; Hu, X.; Larbot, A. *Appl. Catal., A* **2004**, *263*, 171.
(40) Hou, K.; Tian, B.; Li, F.; Bian, Z.; Zhao, D.; Huang, C. *J. Mater. Chem.* **2005**, *15*, 2414.
(41) Huisman, C. L.; Schoonman, J.; Goossens, A. *Sol. Energy Mater. Sol. Cells* **2005**, *85*, 115.

ethanol before deposition onto a copper grid. The environmental ellipsometric porosimetry (EEP) investigations were performed with a Variable Angle Ellipsometer M2000U from Woolam in the range 400−1000 nm by varying the atmosphere relative humidity over the TiO_2 films. The porous volume of TiO_2 films were calculated with the Brugemann Effective Medium Approximation (BEMA) from the optical properties of void and of a TiO_2 reference film prepared without Pluronic F_{127} structuring surfactant with the same thermal history as its mesoporous counterpart. The fractions of porous volume filled with water during the analysis were calculated with BEMA from a mix of the dry mesoporous film and the film completely saturated with water. In parallel, this method allows the determination of Young modulus by analysis of film thickness evolution induced by capillary stress during EEP measurements. A model describing the evolution of the film thickness when capillary stress reversibly contracts the film is obtained by coupling the expression of a modified Kelvin equation and Young-Laplace equation. The transverse Yound moudulus is obtained by fitting the experimantal curve by this model. All the details of experimental setup and data treatments have been previously described in ref 42. The current−voltage ($I-V$) characteristics were measured under illumination through the SnO_2:F side with a Solaronix SA solar simulator using a xenon light source which was focused to deliver 1000 W m^{-2}, the equivalent of one sun at AM 1.5. Each measurement was made simultaneously on five identical prototype cells. The devices were not sealed or otherwise protected. The illuminated active area was 0.25 cm^2.

Results and Discussion

TiO_2 Mesoporous Films Characterizations. The preparation of a complete photovoltaic cell implies a careful optimization of each component of the cell (each layer and each interlayer interface). Indeed, the successful realization of a complete cell involves being able to obtain the best compromise between nanocrystallization of TiO_2 film, pore opening of the mesostructure promoting homogeneous P3OT polymer impregnation, and large TiO_2 network surface area enhancing the solar conversion efficiency. The importance of processing conditions on the porosity, structure, and quality of mesostructured films have been well-demonstrated for inorganic layers prepared by "dip coating".[43−45] The main part of our hybrid solid cell being the "spin-coated" inorganic TiO_2 layer, we took a specific care in analyzing as completely as possible both the crystalline nanostructure and the mesoporous structure of different-temperatures-cured TiO_2 films.

The GI-SAXS measurements were performed on these spin-coated films to determine the mesostructure geometry of TiO_2 films. The Figure 1 exhibits three diffraction diagrams recorded after thermal treatment at 350, 450, and 550 °C. At the lower temperature, we obtained a diffraction pattern characteristic of a *Fmmm* space group corresponding

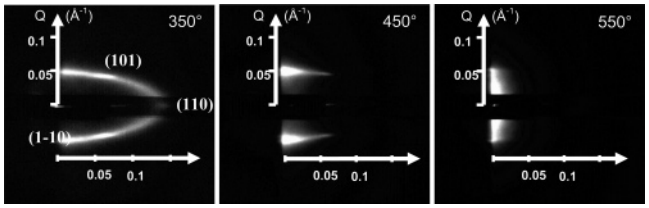

Figure 1. GI-SAXS of TiO_2 films at different temperatures. At 350 °C, the diffraction pattern is characteristic of a *Im*3*m* mesostructure contracted along the [110] direction. Peak attribution is given for the *Im*3*m* referential.

to the uniaxial contraction of a body-centered-cubic structure along its [110] axis.[45,46] The XRD analysis of this film at wide angles exhibited no diffraction peak, indicating that the inorganic domains of the film are amorphous TiO_2 at this temperature. Both results are in agreement with preceding results in the literature.[45] With heating at a temperature higher than 400 °C, the disappearance of the diffraction peaks characteristic of the meso-order in the direction orthogonal to the substrate is observed, concomitantly with the reinforcement of the diffraction peaks in the direction parallel to the substrate. Such transformation, well-documented in the literature as a gridlike transformation, is promoted by the crystallization and diffuse sintering of amorphous TiO_2 into anatase starting between 400 and 500 °C (depending on the pristine thermal history), as was confirmed by wide-angle diffraction measurements shown in Figure 2.[45] The final pore shape is then resulting from the coalescence of each spherical ellipsoid pore with four neighbors. To simplify the pore size measurement, ellipsoidal pores shape has been assumed. The mean crystallite size was calculated from the Debye−Scherrer method at 16 nm.

The final mesostructure was then analyzed by TEM. Figure 3 shows a TEM picture of the 550 °C-calcined TiO_2 film. These observations confirmed that the film is a porous layer resulting in the periodic packing of $10 \times 10 \times 18$ nm^3 anatase nanocrystals with flat crystal−crystal interfaces of about 10×10 nm^2. Large axes of these crystals are aligned and form planes made of parallel polycrystalline anatase "wires". These planes are stacked on each other with a rotation of 90°. The porous network is made of cavities between these polycrystalline anatase "wires". The grain−grain interfaces (very often not well-characterized in the literature of hybrid solar cells) is of paramount importance for the photovoltaic application, being that it strongly influences the transport of electrons within the semiconducting inorganic network. In our case, the flat crystalline interfaces are of the same section as the nanocrystals. Both the gridlike mesostructure and the connecting geometry are assumed close to optimal TiO_2 conductivity, being that the inorganic network contains no conductivity dead end and that the section of electrons diffusion ways is maintained all throughout the film. Hence, the conductivities of both surface and bulk TiO_2 nanocrystals are maintained as constant as possible.

The porous network properties of these films cured at different temperatures were then investigated by EEP technique. From these analyses, TiO_2 films could be fitted

(42) Boissière, C.; Grosso, D.; Lepoutre, S.; Nicole, L.; Brunet-Bruneau, A.; Sanchez, C. *Langmuir* **2005**, *21*, 12362.
(43) Cagnol, F.; Grosso, D.; Soler-Illia, G. J. A. A.; Crepaldi, E. L.; Babonneau, F.; Amenitsch, H.; Sanchez, C. *J. Mater. Chem.* **2003**, *13*, 61.
(44) Grosso, D.; Cagnol, F.; Soler-Illia, G. J. A. A.; Crepaldi, E. L.; Amenitsch, H.; Brunet-Bruneau, A.; Bourgeois, A.; Sanchez, C. *Adv. Funct. Mater.* **2004**, *14*, 309.
(45) Grosso, D.; Soler-Illia, G. J. A. A.; Crepaldi, E. L.; Cagnol, F.; Sinturel, C.; Bourgeois, A.; Brunet-Bruneau, A.; Amenitsch, H.; Albouy, P. A.; Sanchez, C. *Chem. Mater.* **2003**, *15*, 4562.
(46) Falcaro, P.; Grosso, D.; Amenitsch, H.; Innocenzi, P. *J. Phys. Chem. B* **2004**, *108*, 10942.

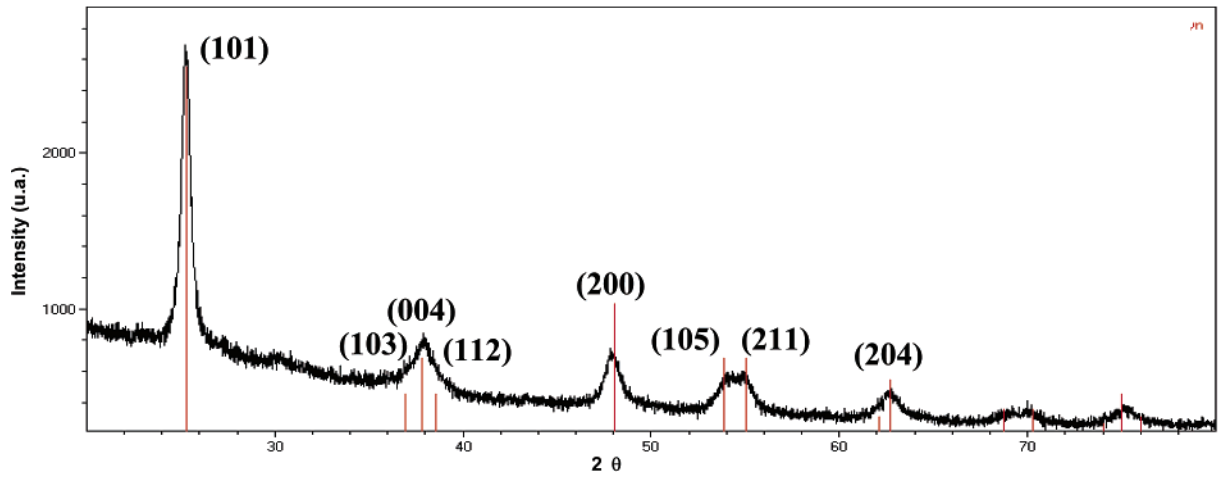

Figure 2. Diffraction patterns measured for the 550 °C-cured TiO_2 film sample ($\omega = 1.4°$) showing the crystallized TiO_2 anatase phase.

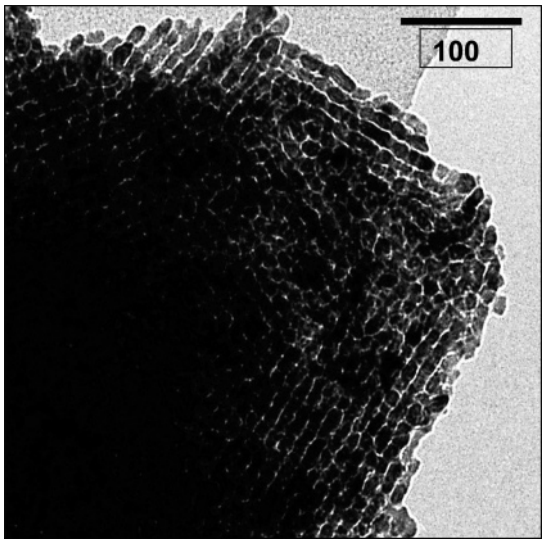

Figure 3. TEM picture of 550 °C-calcined TiO_2 sample. The layer is made of an ordered packing of anatase nanocrystals.

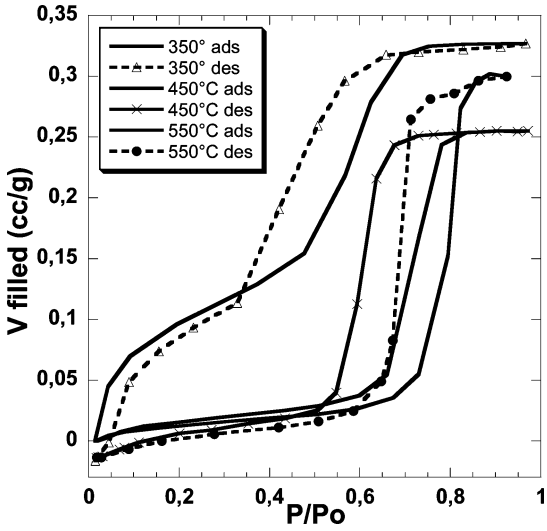

Figure 4. Water adsorption−desorption isotherm of mesostructured TiO_2 at different sintering temperatures.

with a model describing the film as a single homogeneous porous layer with a refractive index much lower than the dense TiO_2. By adsorbing water within the film pores at different relative humidities, we obtained the adsorption−desorption isotherms presented in Figure 4. The 350 °C-calcined TiO_2 films exhibited an isotherm characteristic of a micro- and mesoporous structure with a high porous volume. The capillary adsorption steps, observed at $P/P_o = 0.55$, $P/P_o = 0.73$, and $P/P_o = 0.80$ respectively for films cured at 350, 450, and 550 °C, are very steep and suggest that the mesopore size distribution is narrow in all of the range of temperatures investigated. The analysis of these isotherms with a Kelvin's equation modified for water adsorption[42] led to the evolution of porous parameters of these films with the temperature of calcination (see Table 1). One observed that the film surface area decreased from 493 to 251 $m^2\ cm^{-3}$ during the crystallization. This loss of surface was concomitant with the loss of the major part of microporosity. At this point, one has to notice that, at 450 °C, some residual carbon, coming from the incomplete calcination of the template, is still present within the film (evidenced by FTIR and surface wetting angle measurements not shown here). This carbon disappears with thermal treatment at 550 °C, which totally frees the porosity. The

Table 1. Porous Network Parameters and Young Modulus of Mesoporous TiO_2 Films Calcined at Different Temperatures

thermal treatment	pore large axis (nm)	pore small axis (nm)	porous volume ($cm^3\ cm^{-3}$) micro./meso.	surface area ($m^2\ cm^{-3}$)	Young modulus (GPa)
350 °C	3.9	2.0	0.04/0.29	493	8.12
450 °C	8.0	3.5	0.01/0.26	251	6.50
550 °C	14.0	5.9	0.30	173	1.05
550 °C	14.0	5.9	0.30	173	1.05
600 °C	8.5	4.5	0.30	168	1.26

resulting film exhibits a porous volume of 0.30 $cm^3\ g^{-1}$ and a surface area of 173 $m^2\ cm^{-3}$ with elongated pores (assumed ellipsoidal for the calculation) of parameters $14.0 \times 5.9\ nm^2$. For thermal treatment at temperatures higher than 550 °C, anatase crystals slowly grow by diffuse sintering, the film density increases, and the surface area decreases proportionally with the densification. The mechanical investigation of films obtained by EEP (Young modulus reported in Table 1) gave some interesting results. Indeed, at 350 °C, amorphous TiO_2 films are highly rigid with higher Young modulus ($E = 8.12$ GPa) than those reported for other amorphous inorganic mesoporous layers.[42] At the starting of titania crystallization, the 450 °C-cured film exhibits a slightly smaller E value (6.50 GPa). A sudden decrease of E was

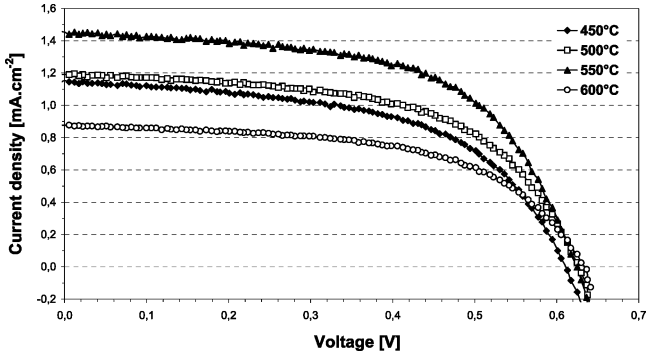

Figure 5. Current−voltage characteristics of dye-sensitized solid solar cells based on mesostructured-anatase TiO_2 films sintered at different temperatures: 450 °C (◆), 500 °C (□), 550 °C (▲), and 600 °C (○) under AM 1.5 illumination (TiO_2 film thickness = 250 nm).

Table 2. Parameters for Current−Voltage Characteristics of the Hybrid Solid-State Solar Cells Using Mesostructured-TiO_2 Films Sintered at Different Temperatures

sintering temperature (°C)	fill factor (FF)	open circuit potential V_{oc} (V)	short circuit current I_{sc} (mA cm^{-2})	energy conversion efficiency η_e (%)
450	54	0.61	1.15	0.38 ± 0.02
500	57	0.62	1.19	0.42 ± 0.03
550	58	0.63	1.42	0.52 ± 0.04
600	57	0.63	0.88	0.32 ± 0.02

observed after calcination at 550 °C with a E value of 1.05 GPa. This change can be easily explained by the full crystallization of the inorganic network which transformed the bulk amorphous monostructure of TiO_2 into a polydomain nanocrystalline suprastructure, exhibiting much less rigidity due to the appearance of the superplasticity property well-known for ceramics prepared by sintering of nanosized metal oxide colloids.[47] This observation points out that even if the nanocrystallization starts between 400 and 450 °C, the full nanocrystallization and the complete percolation of a nanocrystalline network needed for optimized conductivity occurred only at 550 °C.

Influence of Curing Temperature on Energy Conversion Efficiency. We have elaborated and evaluated all solid-state solar cells containing 250-nm-thick mesostructured TiO_2 layers sintered at different temperatures. The goal of this study was to achieve the best compromise between different mesoporous TiO_2 layer features such as mesostructure stability, pores and crystallites size, percolation efficiency, and organic−polymer surface, dye and polymer distribution, and impregnation. The performances of mesostructured anatase/Ru-dye/P3OT photovoltaic devices are presented in Figure 5. The observed $I-V$ plots for anatase films sintered at 450, 500, 550, and 600 °C show strong differences. The best energy conversion efficiency η_e reaches 0.52% for photovoltaic cells built from a 550 °C-sintered mesoporous TiO_2 layer (Table 2). These results have been reproduced on at least five different cells and are in compliance with the values reported by Wang et al.[48]

The mesostructured anatase-based photovoltaic devices present high values of open circuit potential (V_{oc}) and fill factor (FF) (Table 2). TiO_2-layer sintering temperature does not really have an impact either on the fill factor (FF = 54−57) or on the open circuit voltage (V_{oc} = 0.61−0.63 V). In contrast, increasing the densification temperature up to 550 °C leads to an enhancement of short circuit current (I_{sc}) with an maximal value of 1.42 mA cm^{-2}. On the other hand, for photovoltaic cells built from 600 °C-sintered mesoporous titania, a noticeable drop of the energy conversion efficiency is observed. This drop is probably due to a too important mesostructure collapse leading to a more difficult charges transport inside the TiO_2 layer or a decrease of TiO_2 surface area which alters the polymer−dye−TiO_2 interfaces. This result suggests that the best photovoltaic results of our system are obtained when the TiO_2 film exhibits a completely nanocrystallized mesostructure (spotted by Young modulus measurements) and the largest polymer−TiO_2 interface (directly related to the TiO_2 surface area before impregnation). During this study, we did not quantify the exact amount of ruthenium dye and P3OT impregnated within the inorganic mesostructure. In particular, the polymer impregnation step is still to be optimized, attending the high viscosity of the impregnation solution. It should also be highlighted that the present efficiency is limited by the low TiO_2-film thickness (about 250 nm) which is mainly responsible for the small amount of cell-absorbed light. Several routes allowing film thickness increase, such as multilayer deposition or better layer shrinkage control, are currently in progress in our laboratory. However, these initial characteristics values make these nanocrystalline mesostructured TiO_2 films especially attractive for all solid-state dye-sensitized solar cells taking into account that TiO_2-film thickness has not yet been optimized.

Conclusion

Sol−gel chemistry, spin-coating deposition, and thermal curing conditions have been optimized to elaborate porous mesostructured 100% nanocrystalline anatase layers. These titania mesoporous thin films have been structurally and mechanically characterized through the use of complementary techniques such as XRD, GI-SAXS, TEM, and EEP. Our results indicate that these highly crystallized mesoporous TiO_2 layers allow the building of photovoltaic devices that exhibit energy conversion efficiencies (η_e = 0.52% for 250-nm-thick mesostructured TiO_2 layers) comparable to colloidal nanocrystalline anatase films having larger thickness (η_e = 0.02−0.40% for several micrometers thick colloidal anatase layers).[11,18,19,23] The reported energy conversion efficiencies make these mesostructured TiO_2 films very attractive for the designed construction of all solid-state dye-sensitized solar cells. We are currently working on the optimization of P3OT polymer impregnation in mesostructured TiO_2 layer as a function of sintering temperature and on the elaboration of thicker mesostructured anatase layers to improve the response of this new generation of hybrid solar cells.

CM060925Z

(47) Siegel, R. W.; Fougere, G. E. *NATO Nanophase Materials: Synthesis-Properties-Applications*; Kluwer Academic Publisher: Corfu, 1993.
(48) Wang, H.; Oey, C. C.; Djurisic, A. B.; Xie, M. H.; Leung, Y. H.; Man, K. K. Y. C.; Chan, W. K.; Pandey, A.; Nunzi, J.-M.; Chui, P. C. *Appl. Phys. Lett.* **2005**, *87*, 023507.